ISSN 0016-7029, Geochemistry International, 2006, Vol. 44, No. 12, pp. 1225–1236. © Pleiades Publishing, Inc., 2006.
Original Russian Text © Yu.I. Galushkin, M. Makhous, 2006, published in Geokhimiya, 2006, No. 12 pp. 1325–1337.

Contribution of Erosion and Intrusive–Hydrothermal Activity to the Depth Profile of Organic Matter Maturation in Sedimentary Basins

Yu. I. Galushkin[a] and M. Makhous[b]

[a] *Moscow State University, Vorob'evy gory, Moscow, 119992 Russia*
e-mail: gal@mes.msu.ru
[b] *Universite Pierre et Marie Curie, Paris, France*

Received April 19, 2005

Abstract—Sharp variations in organic matter (OM) maturity with depth in sedimentary basins reflected in an abrupt increase in vitrinite reflectance (%Ro) can be caused by both the thermal effect of intrusions accelerating OM maturation in adjacent rocks and removal of a thick sedimentary layer during the extensive erosion of the basin. It is traditionally believed that the erosion of a 1.5–3.0-km-thick sedimentary layer must significantly affect the depth profile of OM maturity, resulting in a drastic increase in %Ro in the present-day sedimentary basin. Some authors used such jumps (ΔRo) to estimate the amplitude of erosion. However, our analysis showed that the depth profile of %Ro is controlled not only by the amplitude of erosion but also by sedimentation history during the posterosion stage of basin evolution. Eastern Algerian basins are good examples to examine this problem, because their evolution involved both the stage of extensive Hercynian erosion and subsequent strong hydrothermal and intrusive activity. Numerous measurements of %Ro in core samples from eastern Algerian sedimentary basins were used to analyze this problem. The calculations of %Ro(z) distributions on the basis of numerical reconstructions of the thermal history of sedimentary sections in more than 60 boreholes of the area showed that the Hercynian erosion could account for only a minor part of the observed amplitude of Δ%Ro, in spite of the significant amplitude of erosion (1.5–3.5 km) typical of the basins of the Algerian Sahara. At the same time, the intrusive and associated hydrothermal activity of the Triassic and Jurassic adequately explains the amplitude of a stepwise increase in OM maturation with depth in the present-day sedimentary sections of these basins. Thus, the reliability of erosion amplitudes estimated from jumps in depth profiles of %Ro can be assessed only after the detailed examination of the posterosion history of the basin.

DOI: 10.1134/S0016702906120068

INTRODUCTION

A sharp stepwise change in the maturity of organic matter (OM) with depth is typical of many sedimentary basins around the world (Urengoi graben in the western Siberian basin [1, 2]; flood basalt province of eastern Siberia [3–6]; Barents Sea shelf basin [7]; Parana basin in Brazil [8]; Oued el-Mya, Ghadames, Illizi, and other basins in the Algerian Sahara [9–15 and others]). Such jumps in vitrinite reflectance (%Ro) with depth can be caused either by the thermal effect of intrusions on OM maturation in the basin or by the removal of a thick sedimentary layer during extensive erosion. The emplacement of an intrusion into the sedimentary cover of the basin results in the development of an OM maturation profile with a rapid decrease in %Ro away from the intrusion. A sharp stepwise increase in %Ro with its subsequent monotonous growth in deeper levels is observed, if an intrusion was emplaced beneath the sedimentary cover, near the basement surface. A step in the distribution of %Ro with depth can be related to the heating of the sedimentary sequence throughout its entire section by a conductive heat flow from the intrusion or by the intrusion-induced convective flow of pore waters within the depth interval from the basement surface to the aquifer.

In addition to the thermal effect of intrusions, a steplike increase in %Ro with depth can be generated in sedimentary sequences that experienced high-amplitude erosion at a certain stage of basin evolution. Such an interpretation of jumps in OM maturation profiles was favored by many authors, when drilling and seismic sounding confirmed the absence of an intrusive body in the sedimentary cover of the basin. For instance, a stepwise 0.5–2.5% increase in %Ro typical of the depth profiles of the Lower Saxonian basin was explained by the erosion of a more than 4-km-thick sedimentary sequence during thermal activation of the basin [16]. It is usually believed that the erosion of a 1.5–3.0-km-thick sedimentary succession must cause a stepwise increase in the modern distribution of %Ro with depth. However, we will show in this paper that a jump in %Ro distribution depends not only on the amplitude of erosion but also, to a considerable degree, on sedimentation history during the posterosion stage

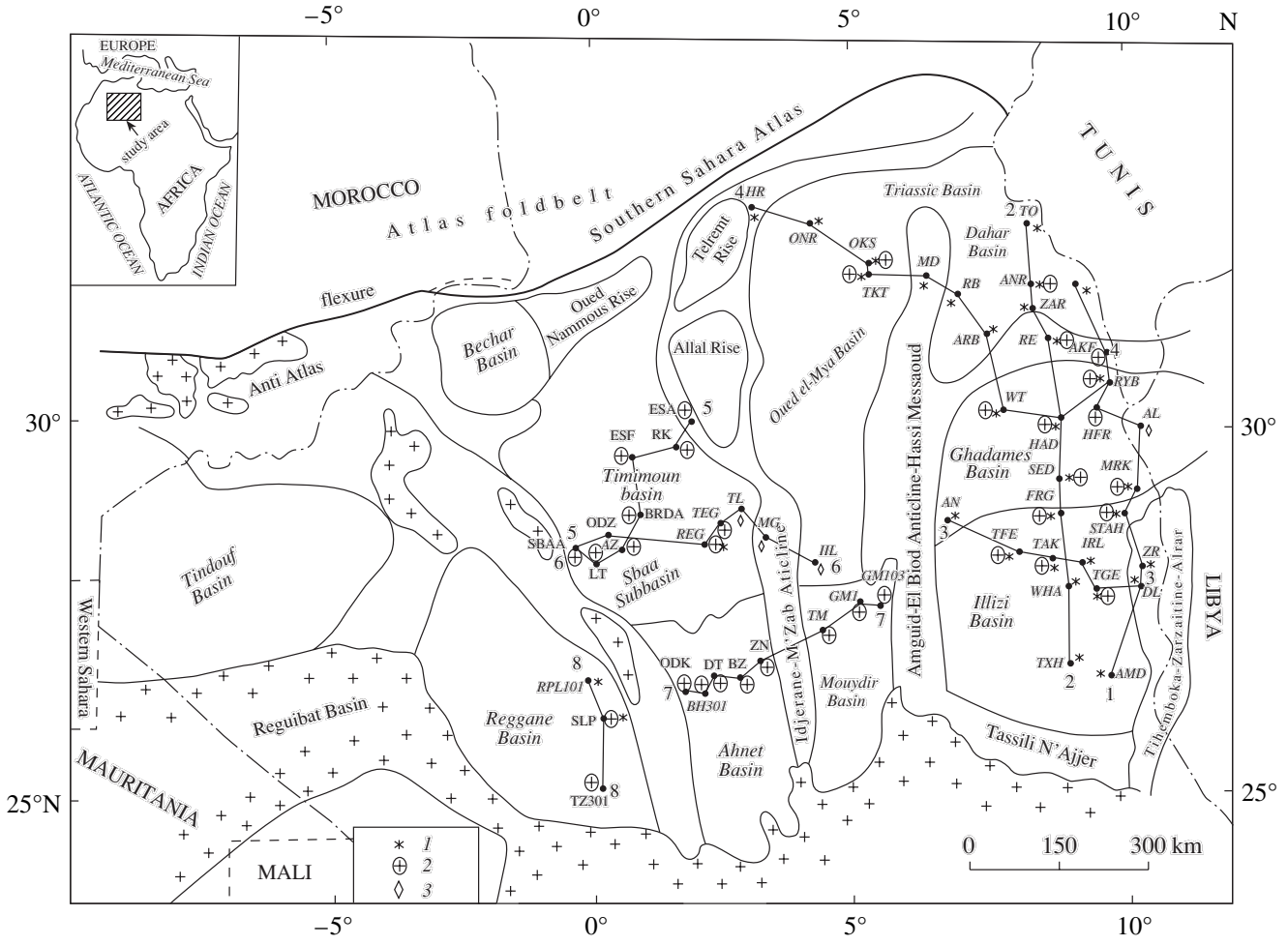

Fig. 1. Position of profiles and oil–gas boreholes. (*1*) Boreholes in which deep temperatures were measured; (*2*) boreholes in which %Ro was measured in core samples; and (*3*) boreholes in which neither temperature nor %Ro was measured. Abbreviations for borehole names: AKF, Akfadou; AMD, Amd; AN, An; ARB, Arb; Dl, Edjeleh; FRG, Frg; GLA, Guellala; HAD, Haid; HFR, Hfr; MD(HMD), Hassi Messaoud; HR, Hassi R'Mel; IRL, Iralene; KA, Keskassa; MRK, Mereksen; OKS, Benkahla; ONR, Oued el-Noumer; RB, Rhourd el-Baguel; RE, Bir Rebaa; RN, Rhourd el-Nouss; RTB, Rhoud el-Yacoub; SED, Sedoukhane; STAH, Stah; TAK, Tak; TFE, Tin Fouye East; TGE, Tiguentourine East; TKT, Takhoukht; TO, To; TXH, Txh; WHA, Wha; WT, Wadi el-The; ZAR, Zar; ZR, Zarzaitine.

of basin evolution. Numerous measurements of %Ro in core samples from the eastern Algerian sedimentary basins are particularly suitable for the evaluation of this problem. In the Saharan basins, strong Hercynian erosion took place simultaneously with intense hydrothermal and intrusive activity. The reconstruction of the thermal evolution of sedimentary sequences in more than 60 boreholes of the area [14, 15] (Fig. 1) showed that the Hercynian erosion accounts for only a minor part of the magnitude of jumps in %Ro in spite of its considerable amplitude (1.5–3.5 km). On the other hand, the intrusive and related hydrothermal activity of the Triassic and Jurassic satisfactorily explains the amplitudes and depths of stepwise increases in OM maturity in the sedimentary basins of the Algerian Sahara.

GEOLOGY

The major geologic structures of the area selected for the analysis of the problem are shown in Fig. 1. They include the basins of the Algerian Sahara (Oued el Mya, Triassic, Dahar, Ghadames, Illizi, Mouydir, Ahnet, Reggane, and Timomoun) and uplifts between them. The geology of the area was discussed in detail with application to the numerical reconstruction of the history of subsidence and thermal regimes of the aforementioned basins [14–18]. Only a brief description is given here, with emphasis on the stages of erosion and intrusive–volcanic activity in the area.

The African plate has been stable over the last 600 Ma, and the West African craton was stabilized 2000 Ma ago. However, many lithospheric faults were formed there in the Late Mesozoic and Cenozoic [19]. For

example, mobile belts surrounding the West African craton experienced several phases of tectonic activation during the Mesozoic and Cenozoic [20]. A gap in the sedimentary succession from the Permian to the Late Triassic is the most significant event in the stratigraphic record of the Atlantic margins of North America and northwestern Africa [21]. The Permian–Triassic thinning of the crust for approximately 75 Ma controlled the position of the spreading axis of the incipient ocean. In the Saharan basins located along the periphery of this area, heating and related thermal expansion of the lithosphere and a shift of phase boundaries caused an uplift of the lithospheric surface and extensive erosion of the region. Faulting, volcanism, and marine transgression at the end of the Middle Triassic event of crustal thinning and movement along strike-slip faults occurred concurrently with events along the Moroccan and Algerian margins of the Tethys. The third stage of the Pangea breakup took place in the Late Triassic, when numerous deep faults were formed and marine transgressions of the Tethys occurred through the northern African margins into the proto-Atlantic basins. This resulted in the deposition of clastic and evaporite sediments. The opening of the Atlantic Ocean in the Late Triassic–Early Jurassic resulted in the dismembering of newly formed continental margins of Africa and North America into small blocks and basins. The subsidence and marine transgressions were accompanied by the deposition of evaporates in areas with partially limited seawater circulation. This time period was marked by the universal emplacement of diabase dike swarms (Anti-Atlas, Algeria, Mauritania, Liberia, Guinea, and the Piedmont Province in eastern North America [21]).

The thermal and tectonic evolution of the southern part of the Saharan basins (Illizi, Ahnet, Mouydir, and Reggane) is closely related to the geologic history of the Hoggar Massif. It is thought that the Hoggar was formed as a shield at the end of the Cretaceous. Its recent history includes two phases. The first of them involved lithospheric extension and lasted from the Early to Middle Cretaceous. It could be responsible for the formation of N–S and NNW–SSE-trending extensional structures and a number of sagging troughs owing to the reactivation of Pan-African faults. This stage could also be related to crustal thinning in central–western Africa as a result of the influence of stress fields induced by the opening of the Central Atlantic. This extensional event produced basaltic volcanism (from tholeiitic to subalkaline) in the eastern Hoggar. The second evolutionary stage of the Hoggar uplift (Late Cretaceous and Cenozoic) corresponded to a change in the stress field owing to the collision between Africa and Europe [22] and resulted in reactivation of NE–SW lineaments as strike-slip faults. Recent magmatic activity in the Hoggar was predated by volcanic activity in the Late Cretaceous and Eocene. The activity of Miocene and Pliocene–Quaternary age gave rise to within-plate alkaline volcanism [23] in many places of the uplift. This activity could be related to the anomalous upwelling of the upper mantle boundary in the Late Cretaceous–Eocene.

Magmatism is a characteristic feature of the geologic history of the Algerian Sahara. The Phanerozoic alkaline magmatism of Africa culminated during widespread rifting in the Early Mesozoic, which preceded the breakup of Gondwana. Basaltic eruptions peaked in the Late Triassic–Early Jurassic and resumed in the Late Cenozoic during the formation of the East African rift system owing to reactivation of deep faults. Pyroclastics disrupted by supposedly Quaternary volcanic activity are preserved in the Cretaceous deposits of the northeastern part of the Illizi basin [24]. Volcanoes are aligned along NE-trending faults and presumably represent a northern continuation of the similar structures of the Hoggar Massif. On the other hand, recent calc-alkaline (andesitic) volcanism in the northern Saharan platform (Alpine area) was presumably related to a zone of underthrusting, which was completed in the early Pliocene [11, 12].

JUMPS IN THE DISTRIBUTIONS OF OM MATURITY WITH DEPTH IN THE ALGERIAN SAHARAN BASINS

The numerical reconstruction of the burial history and thermal evolution of the Algerian Saharan basins [14, 15] made it possible to calculate the OM maturity of basin rocks, including its variations with depth and time. The value of %Ro was calculated using the EASY%Ro kinetic model, which describes the process of vitrinite maturation by 20 first-order Arrhenius reactions. The degree of vitrinite transformation, $Tr_1(t)$, can be calculated by the expression

$$Tr_1(t) = \sum_1^n X_{i0}\left\{1 - \exp\left[-\int_{t_0}^{t} K_i(t')dt'\right]\right\}, \qquad (1)$$

where $K_i(t) = A_i\exp[-Ei/(RT(t))]$ is the rate of the ith reaction, A_i is the frequency factor, X_{i0} is the initial potential, Ei is the activation energy, and $T(t)$ is the temperature history of the sample for which the OM maturity (%Ro) is calculated or measured. The values of A_i, X_{i0}, and Ei were reported in [25]. The values of vitrinite reflectance can be determined from the degree of transformation, $Tr_1(t)$, using the relation [25]

$$Ro\% = EXP\,[-1.6 + 3.7\,Tr_1(t)]. \qquad (2)$$

Figures 2 and 3 show variations in the calculated %Ro values with depth in the modern sequences of the Algerian Saharan basins and the measured values of vitrinite reflectance. Temperature variations, $T(t)$, during the burial history of the rocks of the basins, which are required to calculate the degree of transformation by

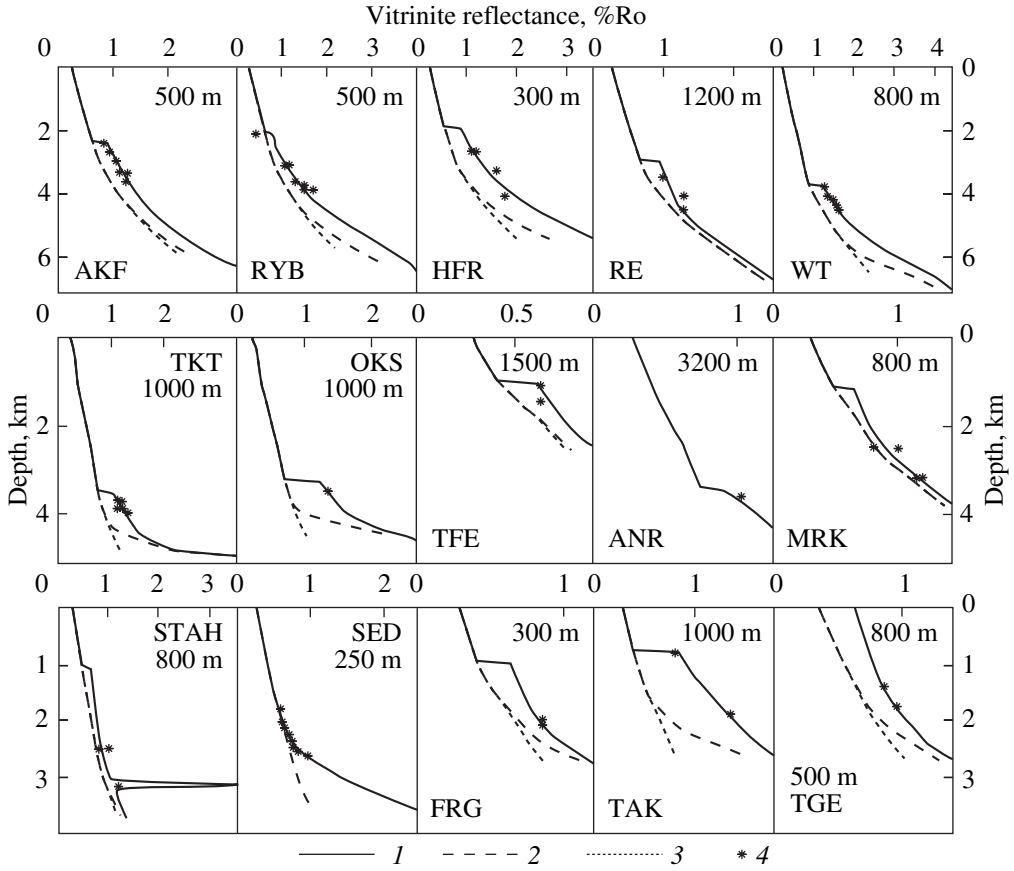

Fig. 2. Distribution of vitrinie reflectance (%Ro) with depth in the modern sedimentary basins of the eastern and western Sahara [14, 15]. (*1*) %Ro calculated accounting for heating of the rock due to its burial in the basin, thermal influence of an intrusive, and hydrothermal flow (see text); (*2*) the same, without considering hydrothermal heating; (*3*) the same, without considering conductive heat transfer from the intrusion and hydrothermal heating (regional level of maturity, see text); and (*4*) measured %Ro. The position of areas is shown in Fig. 1.

Eq. (1), were obtained from the reconstruction of the thermal evolution of the Algerian basins by the procedure of basin modeling described in [14, 15]. The following input parameters were used in this modeling: the modern sedimentary sequence of the basin, estimated amplitudes and rates of erosion, lithology and thermophysical properties of the sedimentary rocks and basement, structure and composition of the basin lithosphere, estimates of OM maturity (vitrinite reflectance, %Ro), paleoclimate and paleodepths, measurements of heat flow and temperatures, and geological and geophysical information on the evolution and modern tectonic conditions of the area [14, 15]. The plausibility of numerical basin reconstructions, which were used to calculate profiles in Figs. 2 and 3, was checked by comparing the calculated and measured values of deep temperatures and vitrinite reflectance (Fig. 4), as well as by the analysis of variations in tectonic subsidence of the basement. The latter parameters were calculated with due allowance for density variations in basement rocks, which were caused by the heating or cooling of lithospheric rocks during the thermal activation or cooling of the basin, crustal thinning owing to lithospheric extension, shift of phase boundaries in the mantle, etc. [1, 14–18, 26].

Figure 5 shows the results of numerical reconstructions of basin evolution for profile 2 (Fig. 1), and Fig. 6 presents the same data for sedimentary sections in the vicinity of the ANR-1 and REG-1 boreholes (Fig. 1). These reconstructions illustrate the most characteristic features of the thermal evolution of the Algerian Saharan sedimentary basins. The most prominent among them are the intense deposition of sediments in the Devonian and Cretaceous and significant erosion expressed as Hercynian unconformities in all sections of the area. For areas along profile 2 (Fig. 5), the amplitude of Hercynian erosion can be estimated by comparing the thicknesses of the 322 and 255 Ma sections. The erosion was changed and in part accompanied by hydrothermal and intrusive activity in the Triassic and Early Jurassic, the numerous indications of which were considered in [14, 15].

A characteristic feature of the %Ro depth profile in the basins of the eastern (Fig. 2) and western (Fig. 3)

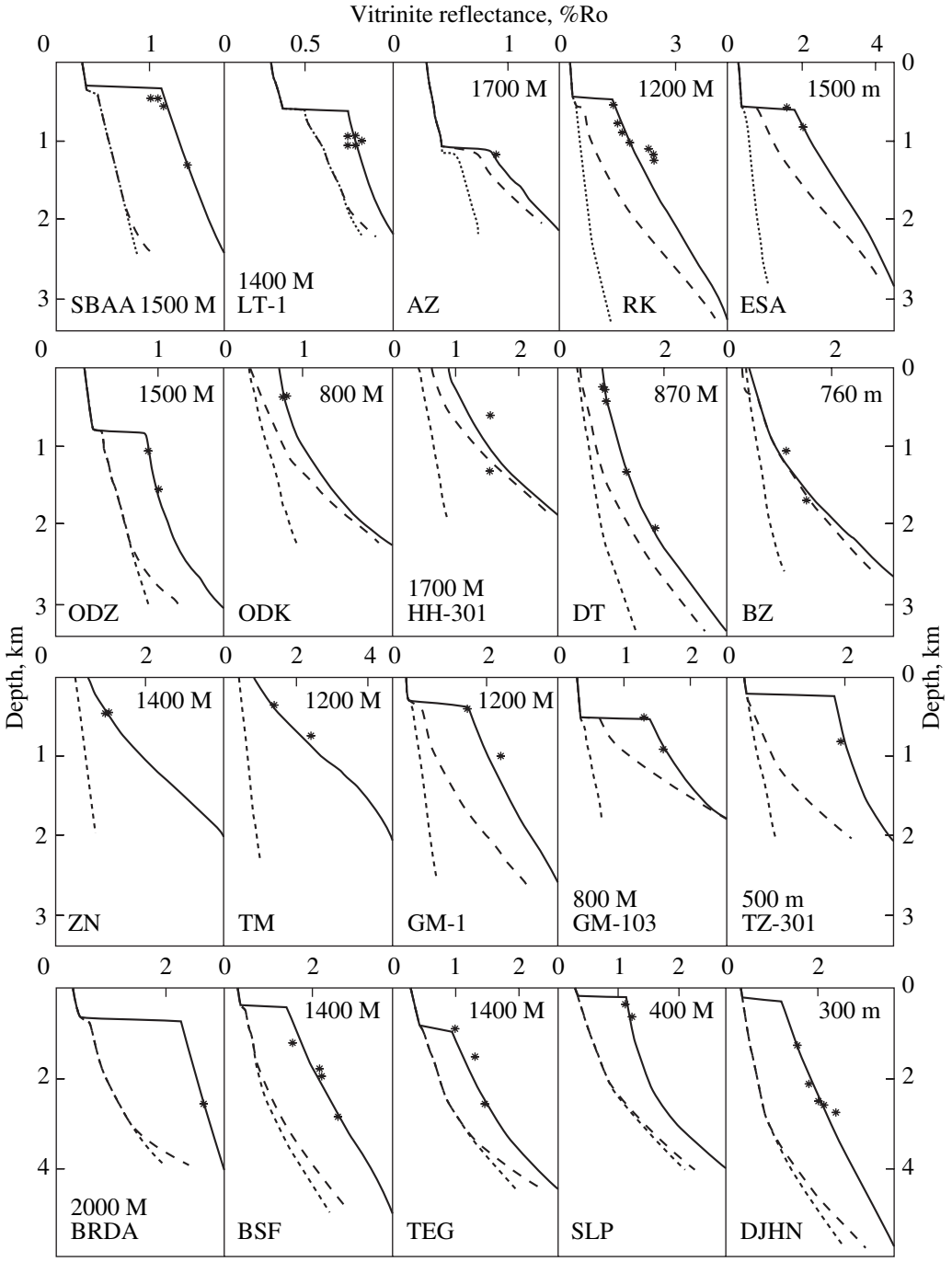

Fig. 3. Distribution of vitrinite reflectance (%Ro) with depth in the modern sedimentary basins of the southwestern Sahara. Symbols are the same as in Fig. 2. The position of areas is shown in Fig. 1.

Algerian Sahara is a stepwise increase in the degree of OM maturity. In order to compare the contributions of erosion, conductive, and convective heat transfer from intrusions to variations in the distribution of OM maturity with depth, three types of %Ro depth profiles are shown in Figs. 2 and 3 by solid, short-dashed, and long-dashed lines, respectively. The short-dashed lines represent %Ro profiles obtained ignoring the local thermal influence of the intrusive and hydrothermal activity in the Triassic–Jurassic and illustrate the effect of erosion on the development of %Ro depth profiles. They correspond to the regional level of OM maturity (shown by %Ro isolines in Fig. 5 and for the borehole ANR-1 in Fig. 6). The %Ro profiles shown by solid lines in Figs. 2 and 3 were calculated taking into account the local thermal influence of intrusive and hydrothermal activity

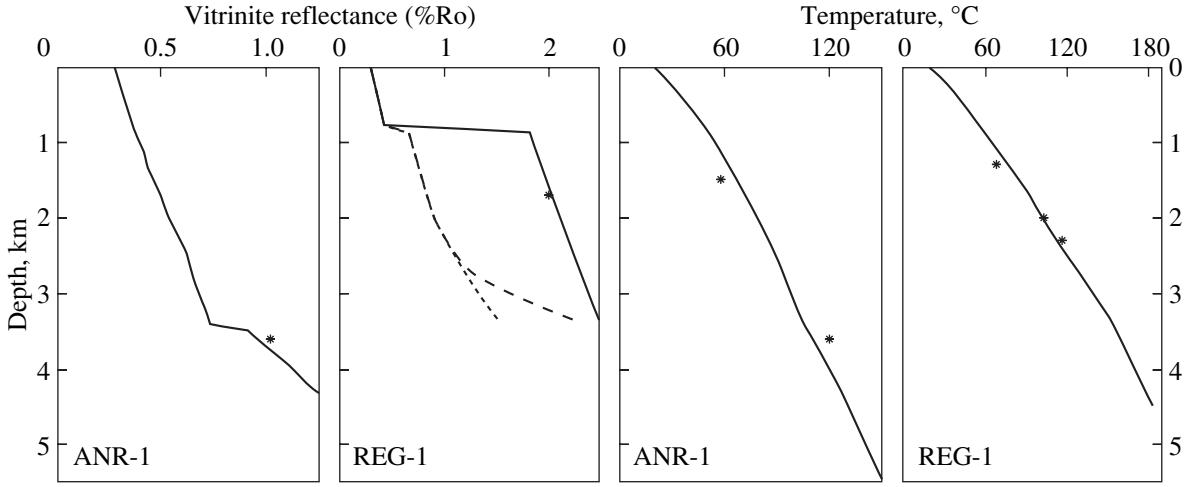

Fig. 4. Variations of vitrinite reflectance and temperature in the sedimentary sections of the ANR-1 borehole in the Dahar Basin and the REG-1 borehole in the Timimoun basin. Symbols are the same as in Fig. 2. The ANR area is one of a few areas in the study region, in which variations in %Ro with depth in the modern section can be explained without invoking heating by intrusions.

and correspond to the distribution of %Ro(z) in the modern basin. The profiles shown by long-dashed lines were calculated ignoring the thermal effect of hydrothermal activity but accounting for variations in OM maturity under the influence of conductive heat transfer from intrusions. Thus, a comparison of the solid and long-dashed lines makes it possible to estimate the contribution of hydrothermal heat transfer to the %Ro(z) profile, and a comparison of short-dashed and long-dashed lines provides insight into the contribution of conductive heating by intrusions. The three curves, solid, short-dashed, and long-dashed ones, coincide at depths corresponding to the Jurassic and younger rocks, when no significant intrusive and erosion activity occurred in the basin but are significantly different below the Hercynian unconformity.

ROLE OF EROSION IN THE DEVELOPMENT OF OM MATURITY VARIATIONS IN BASIN ROCKS WITH DEPTH

Figures 2 and 3 may give the impression that the stepwise increase in %Ro with depth in the Algerian Saharan basins was mainly caused by the Hercynian erosion. However, there is no correlation between the erosion amplitudes shown in meters in Figs. 2 and 3 and the magnitude of jumps, ΔRo. The true contribution of Hercynian erosion to the %Ro(z) profile can be assessed by comparing the solid and short-dashed %Ro profiles in Figs. 2 and 3. As was mentioned above, the latter profiles reflect the regional distribution of OM maturity, i.e., the distribution calculated without considering local heat effects due to intrusive and hydrothermal activity. In such a case, a jump in %Ro(z) can be caused by erosion only. As can be seen in Figs. 2 and 3, the only sedimentary section in which a jump in the %Ro(z) profile can be explained by the Hercynian erosion without intrusive heating is that of the ANR borehole. But even in that case, the jump magnitude, ΔRo, is as low as 0.2%, in spite of the high estimated value of erosion amplitude (3200 m). For other sections in Figs. 2 and 3, the contribution of Hercynian erosion was either very small or negligible, although the erosion amplitude could reach 1700 m. Thus, the numerical modeling of basin evolution shows that, in spite of the high amplitude of erosion, its effect on the depth profile of OM maturity was probably limited. This result is contrary to the widespread opinion that intense erosion is the main reason for a sharp increase in OM maturity with depth. For instance, Petmecky et al. [16] explained considerable jumps in ΔRo = 0.5–2.5% in the modern section of the Saxonian basin by erosion of more than 4200 m in combination with a high heat flow (more than 70 mW/m^2) during the preerosion evolution of the basin.

Using relatively simple examples, we attempted to understand the reasons for such contrasting estimates of the role of erosion in the development of the depth profile of OM maturity. In order to facilitate our analysis, the level of OM maturation was approximately estimated from the temperature–time index [27]

$$TTI = \int_{t_0}^{t_1} 2^{F(T)} dt \qquad (3)$$

where t_0 is the deposition time of the rock on the basin surface, t_1 is the current time, T(t) is the temperature of the rock as a function of time t during the burial evolution of the basin, and

$$F(T) = n - 10 \text{ for } 10n \le T(^\circ\text{C}) \le 10(n+1). \qquad (4)$$

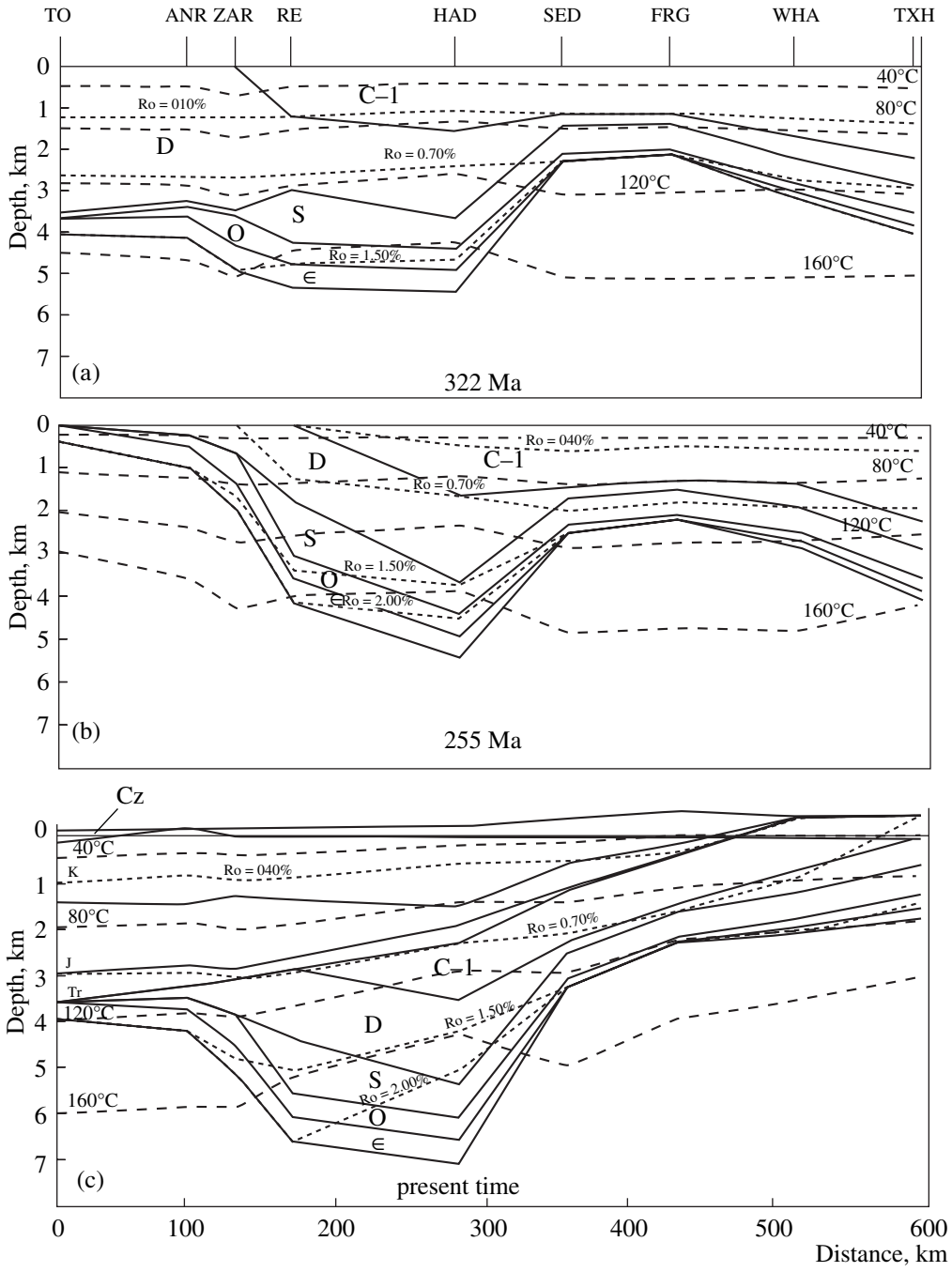

Fig. 5. Numerical reconstruction of the burial history and variations in temperature and maturity in the sedimentary section of the basins of northern and eastern Africa along profile 2. Reconstructions for (a) 322 Ma, (b) 255 Ma, and (c) present time are shown. The depths of %Ro isolines show the regional level of maturity calculated without considering local thermal contribution of intrusions and hydrothermal activity to the profile of %Ro (see text for explanation). The position of the profile and boreholes is shown in Fig. 1.

Expression (3) suggests that the reaction rate of OM maturation is doubled every 10°C increase in temperature [27]. Although Eq. (3) could lead to errors in %Ro values compared to the more accurate kinetic methods [25] used in the reconstructions shown in Figs. 2–6, its accuracy is sufficient for our analysis, and its obvious advantage is the additivity of *TTI* with respect to time. The *TTI*–%Ro correlation after [28] can be used to change from *TTI* to %Ro values

$$(\mathrm{Ro}\%) = -0.4769 + 0.2801\log_{10}(TTI) - 0.007472[\log_{10}(TTI)]^2. \quad (5)$$

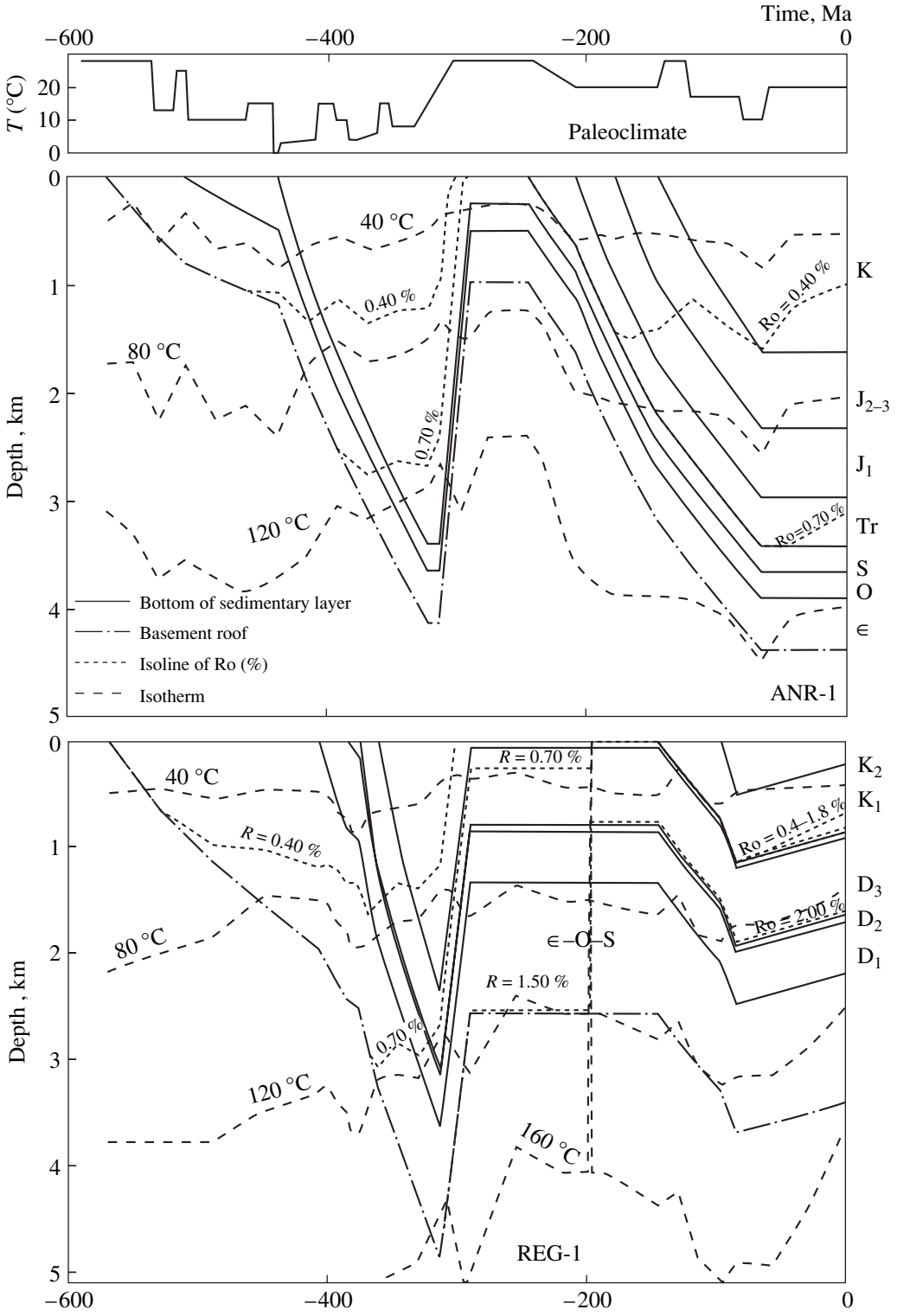

Fig. 6. Numerical reconstruction of burial history and variations in temperatures and maturity for the sedimentary section of basins in the ANR-1 borehole area of the northern Sahara and the REG-1 borehole area of the southern Sahara. In the section of the ANR-1 borehole, the %Ro isolines show the regional level of OM maturity (without influence of intrusions, see text), whereas the isolines for borehole REG-1 characterize the local level of OM maturity calculated taking into account contributions from intrusive heat and hydrothermal activity to the %Ro(z) profile. The positions of the profile and boreholes are shown in Fig. 1.

During our analysis, Eq. (3) was used in two simplest situations: (a) deposition of sediments at a constant temperature gradient and (b) OM maturation under a constant rock temperature. In the former case, the temperature of rock (T) linearly varies with depth:

$$T(\mathrm{t}) = T_0 + \gamma V \mathrm{t}, \quad (6)$$

where T_0(°C) is the average temperature on the basin surface, γ (°C/km) is the constant temperature gradient, and V (km/Ma) is the average rate of sediment deposition for the time interval (0, t). As follows from Eqs. (6) and (3), the precipitation of sediments with the rate V for the time interval Δt (Ma) results in a *TTI* increase by

$$\Delta TTI = \frac{10 \times 2^{T_0/10}}{2^{10}\ln 2\gamma V}\left[2^{\frac{\gamma V \Delta \mathrm{t}}{10}} - 1\right]. \quad (7)$$

If erosion was relatively rapid and the temperature of rocks before erosion was described by Eq. (6), the erosion of a sedimentary layer with a thickness of Δz (in km) will cause a stepwise increase in the degree of maturity on the basin surface equal to

$$\Delta TTI_{\mathrm{erosion}} = \frac{(10 \times 2^{T_0/10})\Delta \mathrm{t}}{2^{10}\ln 2\gamma \Delta z}\left[2^{\frac{\gamma \Delta z}{10}} - 1\right], \quad (8)$$

where T_0 and γ are the parameters characterizing the preerosion period of basin evolution, and Δt is the duration of the deposition of a Δz-thick layer. If an increase in the degree of maturity, ΔTTI, was caused by the exposure of rocks to the average temperature $T = T_{\mathrm{av}}$ for a certain time interval, Δt, (which is similar to a sedimentation gap), an increase in *TTI* according to Eq. (3) is

$$\Delta TTI_{\mathrm{gap}} = \left[2^{\frac{T_{\mathrm{av}}}{10} - 10}\right]\Delta \mathrm{t}, \quad (9)$$

where T_{av} is in °C and Δt is in Ma. This equation suggests that a sedimentation gap exerts a negligible influence on the maturity of rocks, if they were moved by erosion into the near-surface levels of the basin; however, it can significantly affect this parameter for deep-seated rocks occurring under high T_{av}.

Using Eqs. (8) and (9), we attempted to estimate the amplitude of a jump in %Ro(z) for the sedimentary section of the Dahar basin in the area of the ANR borehole, where the maximum erosion amplitude was observed (Figs. 2, 4–6). The values of Δz, Δt, γ, T_{av}, and T_0 in Eqs. (8) and (9) were taken in accordance with the results of numerical modeling (Fig. 6a). The erosion of a layer with a thickness of Δz = 3.2 km, which was precipitated at an average temperature of T_0 = 10°C and γ = 40°C/km, which is typical of the time interval Δt = 103 Ma before erosion, yields according to Eq. (8) $\Delta TTI_{\mathrm{erosion}} \approx 162$ or, according to Eq. (5), ΔRo (erosion) ≈ 1.27%. Hence, according to the *TTI* method, the rocks of the sedimentary section of the ANR borehole brought to a subsurface level by the end of Hercynian erosion have Ro ≈ 1.27%. A jump in ΔRo by approximately 1.27% at the Hercynian unconformity surface would have preserved up to now, if the subsequent stages involving intense sedimentation in the Triassic–Jurassic and a gap in the Cenozoic (Fig. 6a) were absent. Sediment accumulation in the Triassic, Jurassic, and Cretaceous resulted in the subsidence of the Hercynian unconformity to a depth of more than 3000 m. According to Fig. 6a, this period can be characterized by the precipitation of a sedimentary layer with a thickness of Δz = 3.4 km within the time period Δt = 183 Ma at a surface temperature of $T_0 \approx$ 10°C and an average temperature gradient of $\gamma \approx$ 32°C/km. An increase in the degree of OM maturity during that time can be estimated from Eq. (8) as $TTI_{\mathrm{sedim}} \approx 89$. Hence, after Triassic–Cretaceous sedimentation, the rocks above the Hercynian unconformity had $TTI = \Delta TTI_{\mathrm{sedim}} \approx 89$, which, in accordance with Eq. (5), corresponds to Ro (sed) ≈ 1.1%. At the same time, the rocks beneath the Hercynian unconformity showed $TTI \approx 162 + 89 = 251$, which corresponded to Ro ≈ 1.42%. Thus, the precipitation of sediments on the unconformity surface reduced the value of ΔRo at the surface from ΔRo = 1.27% immediately after erosion to ΔRo = 0.32% by the end of the Cretaceous. The subsequent sedimentation gap in the Cenozoic with an average rock temperature of $T_{\mathrm{av}} \approx$ 105°C at the unconformity depth promoted an increase in the degree of OM maturity by $\Delta TTI_{\mathrm{interrup}} \approx 92$ [Eq. (9)]. As a result, the rocks of the modern sedimentary sequence above the unconformity will be characterized by *TTI* = 89 +92 = 181 or Ro ≈ 1.31%, whereas the rocks directly underlying the Hercynian unconformity have $TTI \approx 251 +$ 92 = 343 or Ro ≈ 1.53%. Thus, our simplified analysis showed that the sedimentation and subsequent gap, which occurred after the erosion of a 3.2-km-thick sequence in the Permian, led to a decrease in the amplitude of the jump in the %Ro depth profile at the Hercynian unconformity surface from ΔRo = 1.27% immediately after erosion to ΔRo = 0.22% in the modern section. It is interesting that the latter value calculated by the approximate method is not very different from more accurate calculations shown in Figs. 2 and 4, although the absolute values of %Ro are distinctly different.

Let us perform the same analysis for the sedimentary section of the REG-1 borehole, which exhibits one of the largest ΔRo values (Figs. 2–4, 6b). Assuming, in accordance with Fig. 6b, that the sedimentary layer with a thickness of Δz = 2.3 km was deposited at T_0 = 10°C and γ = 45°C/km in the preerosion period Δt = 49 Ma (Fig. 6b), we obtain the jump ΔTTI = 17.4 or ΔRo ≈ 0.73% at the unconformity surface immediately after erosion. Cretaceous sedimentation at T_0 = 10°C and γ = 50°C/km produced a sedimentary bed with Δz = 0.8 km within Δt = 85 Ma, which yielded $\Delta TTI_{\mathrm{sedim}} \approx 0.9$. The subsequent 65 Ma gap in the Cenozoic with an average temperature at the unconformity surface of $T_{\mathrm{av}} \approx$ 50°C (Fig. 6b) provided $\Delta TTI_{\mathrm{interrup}} \approx 2.0$. Thus, we obtain TTI = 2.9 or Ro = 0.45% for the rocks overlaying the unconformity and *TTI* = 20.3 or Ro = 0.753% for the rocks immediately beneath the Hercynian unconformity. In this case, the contrast

between %Ro values at the unconformity surface caused by the erosion of 2.3 km of sediments in the Permian decreased from $\Delta Ro = 0.73\%$ at the end of the erosion period to $\Delta Ro = 0.30\%$ in the modern section. Thus, using simple examples and approximate relations [Eqs. (5), (8), and (9)], we showed that the influence of erosion on the present-day %Ro profile depends not only on the amplitude of this erosion but also to a considerable extent on the subsequent history of the basin.

INCREASE IN THE DEGREE OF OM MATURITY UNDER THE INFLUENCE OF INTRUSIVE AND HYDROTHERMAL ACTIVITY IN A BASIN

A comparison of %Ro profiles shown by solid and short-dashed lines in Figs. 2 and 3 and the results of approximate analysis from the previous section suggest that the Hercynian erosion in the Algerian basins can explain only a minor portion of jumps in the %Ro(z) profiles. Hence, the most probable mechanism of the formation of such jumps is hydrothermal and intrusive activity, which was similar to the Triassic and Early Jurassic activity in the western Siberian basin resulting in a stepwise increase in the degree of OM maturity in the lower parts of the sedimentary section of the Urengoi field [1]. Numerous pieces of evidence supporting intrusive and hydrothermal activity in the Triassic and Jurassic in the Algerian Saharan basins were reported in [14, 15]. These data suggest that the mechanism of thermal influence on the profile of OM maturation is important for the sedimentary basins of this region. The absence of %Ro measurements above the Hercynian unconformity hampers the accurate determination of the time of the impact of intrusive–hydrothermal activity; however, geological data [14, 15] suggest that these events occurred in the Middle Triassic in the eastern Saharan basins and in the Late Triassic–Jurassic in the western Saharan basins, which is consistent with the age of volcanism in the region [18].

As was mentioned above, the distribution of temperature around an intrusion is controlled, on the one hand, by conductive heat transfer during the cooling of the intrusive body and, on the other hand, by heat transfer related to the hydrothermal convection of pore waters induced by the emplacement of the hot intrusive body into the sedimentary sequence or the upper portion of the basement. In the reconstructions shown in Figs. 2 and 3, the conductive component of the thermal influence of an intrusion on the host rocks was modeled by the substitution of temperatures calculated during basin modeling by the temperature of the intrusion (700–1000°C) within the width of the emplaced intrusion at every time interval of its activity. Figures 2 and 3 show the results of modeling for the emplacement of 100–500-m-thick intrusive bodies (sills) at depths from 100 to 5000 m beneath the basement surface. It should be noted that only one magmatic body was found within the sedimentary cover of the basins. This body was penetrated by the STAH borehole in profile 1 (Fig. 2). During modeling, the depth of emplacement, thickness, and operation time of an intrusion were selected in such a way as to minimize the difference between the calculated profile and the measured values of %Ro. As was mentioned above, the contribution of conductive heat flow from the intrusive body to the %Ro increase can be estimated by comparing the long-dashed and short-dashed lines in Figs. 2 and 3. This comparison clearly shows that in most cases conductive heat transfer alone cannot explain the stepwise increase in %Ro with depth. Exceptions are the sedimentary sections of the ZN, TM (Fig. 3), and SED boreholes (Fig. 2). In the latter case, the emplacement of a 400-m-thick sill with a temperature of 1000°C at a depth of 2 km beneath the basement surface could be responsible for the observed %Ro(z) profile without any contribution from hydrothermal activity. For all other profiles in Figs. 2 and 3, hydrothermal heat transfer was required to provide the consistency between the calculated and measured Ro values in the modern sedimentary section.

The simulation of temperature distribution in the presence of hydrothermal heat transfer is a difficult problem, primarily because of large uncertainties in the distribution of permeability and porosity of rocks with depth [29–31]. In order to circumvent this difficulty, we do not consider the convective heat and mass transfer itself and simulate only its influence on OM maturation. It is known that this process is mainly affected by an increase in temperature gradient within the depth range of hydrothermal activity. When the effect of hydrothermal activity on the %Ro(z) profile was simulated, the existing temperature distribution was changed by a linear "hydrothermal" distribution at each time step of the procedure within the depth interval of hydrothermal activity $z_1 \le z \le z_2$ [1]:

$$T_{hydr}(z, t) = T(z_2) - \Delta T[(z_2 - z)/(z_2 - z_1)]. \quad (10)$$

The new values of the depth boundaries of the zone of hydrothermal activity, z_1 and z_2, and the temperature jump within this zone, ΔT, were chosen in such a way as to obtain consistency between the measured and calculated %Ro values. The duration of hydrothermal heating was taken to be similar to the time of the active existence of the intrusion. The lower boundary of the zone of hydrothermal activity was usually located 0.5–2.5 km above the basement surface and only occasionally coincided with it (STAH, TGE, and TAK boreholes). The upper boundary of the hydrothermal zone typically coincided with the basin surface at any given moment of its evolution. For example, ΔT in Eq. (10) varied from 30 to 60°C for the sedimentary sections shown in Fig. 2. As can be seen in Figs. 2 and 3, abrupt stepwise changes in the degree of OM maturity with depth, which are typical of the intrusive activity zones, can be explained only by invoking the thermal effect of hydrothermal flows induced by the emplacement of magmatic bodies into the upper layers of the basement.

We complete this section by noting that our simulation of the thermal effect of intrusions on the develop-

ment of %Ro(z) profiles shown in Figs. 2 and 3 presents only one of the possible solutions to the problem and cannot be considered as an unambiguous estimation of the parameters of intrusive–hydrothermal systems. The same %Ro(z) profile can be modeled using other characteristics of an intrusion, including its width, temperature, depth, and time of emplacement [1]. However, this must not affect the main conclusions of this study on the relative effects of conductive and convective heat transfer mechanisms on the development of the depth profile of OM maturity in basins. More detailed characteristics of intrusive systems can be obtained by decreasing the step of the difference grid in depth and time during the solution of corresponding heat transfer equations and, more importantly, by utilizing a more detailed grid of Ro measurements around intrusions, similar to that used by us for the analysis of comprehensively dated intrusions [32, 33].

CONCLUSIONS

It is traditionally believed that the erosion of a thick sedimentary layer (1.5–3.0 km) produces a sharp stepwise increase in vitrinite reflectance, %Ro, at the depth of the unconformity surface. Some authors used the values of ΔRo to assess the magnitude of erosion. Our study showed that such estimates must be considered with caution, because the effect of erosion on the depth profile of %Ro depends not only on the erosion amplitude but also, to a considerable degree, on the history of sedimentation during the posterosion stage of basin evolution. The examination of more than 60 sedimentary sections of the Algerian Sahara showed that Hercynian erosion could explain only a small part of the observed ΔRo jump, whereas the intrusive and related hydrothermal activity of the Triassic and Jurassic is well consistent with the amplitude of jumps in the %Ro(z) distribution in these basins.

ACKNOWLEDGMENTS

This study was financially supported by the Russian Foundation for Basic Research, project no. 04-05-64868.

REFRENCES

1. Yu. I. Galushkin, O. I. Simonenkova, and N. V. Lopatin, "Effect of the Giant Gas Pool Formation on the Thermal Regime of Sedimentary Sequence at the Urengoi Field in the West Siberian Basin," Geokhimiya, No. 12, 1335–1344 (1999) [Geochem. Int. **37**, 1203–1211 (1999)].
2. A. E. Kontorovich, I. I. Nesterov, F. K. Salmanov, et al., *Oil and Gas Geology of Western Siberia* (Nedra, Moscow, 1975) [in Russian].
3. M. L. Verba and A. B. Alekseeva, "Effect of an Intrusion on the Bitumen Content of the Host Paleozoic Carbonate Rocks of the Norilsk District," in *Problems of Geology and Oil and Gas Potential of the Tungusska Syneclise*, Tr. Vses. Nauch.-Issled. Geol. Inst., No. 308, 124–142 (1972).
4. V. V. Kazarinov and A. V. Khomenko, "Effect of Traps on the Paleozoic Oil- and Gas-Generating Rocks of the Tungusska and Lena Region," in *Lithology and Geochemistry of Oil–Gas-Bearing Sequences of the Siberian Platform* (Nauka, Moscow, 1981), pp. 113–117 [in Russian].
5. A. E. Kontorovich, I. I. Likhanov, V. V. Lepetyukha, et al., "Application of Geothermometers for the Estimation of Metamorphic Temperatures in Sedimentary Basins with Trap Magmatism," Dokl. Akad. Nauk **345**, 793–796 (1995).
6. E. N. Rodnova, "Change of Collector Properties of Sediments at the Contact with Traps in the Central Part of the Tungusska Syneclise," in *Problems of Geology and Oil and Gas Potential of the Tungusska Syneclise*, Tr. Vses. Nauch.-Issled. Geol. Inst., No. 308, 118–133 (1976).
7. I. S. Gramberg, N. K. Evdokimova, and O. I. Suprunenko, "Catagenetic Zoning of the Sedimentary Cover of the Barents Sea Shelf with Applications to Oil and Gas Potential," Geol. Geofiz. **42**, 1808–1820 (2001).
8. J. A. Triguis and L. M. Arano, "Parana Basin-Brazil: A Huge Pyrolyser. Comparison between Molecular Distributions in Pyrolysed Samples and Source Rocks Affected by Igneous Intrusions," in *Organic Geochemistry: Developments and Applications to Energy, Climate, Environment, and Human History*, Ed. by J.O. Grimalt and C. Dorronsoro, (EAOG, 1995), pp. 512–514.
9. J. Conrad, "Distension Jurassique et tectonique ecocretace sur le nord-ouest de la plateform-Africaine (Bassin de Reggane)," C. R. Acad. Sci. Paris **274**, 2423–2426 (1972).
10. J. Conrad and M. Westphal, *Gondwana Geology* (Australian National University, Canberra, 1975).
11. A. Lesquer, A. Bourmatte, and J. M. Dautria, "Deep Structure of the Hoggar Domal Uplift (Central Sahara, South Algeria) from Gravity, Thermal and Petrological Data," Tectonophysics **152**, 71–87 (1988).
12. A. Lesquer, A. Bourmatte, and J. M. Dautria, "First Heat Flow Determination from the Central Sahara: Relationship with the Pan-African Belt and Hoggar Domal Uplift," J. Afr. Earth Sci. **9** (1), 41–48 (1989).
13. A. Lesquer, D. Takherist, J. M. Dautria, et al., "Geophysical and Petrological Evidence for the Presence of an 'Anomalous' Upper Mantle beneath the Sahara Basins (Algeria)," Earth Planet. Sci. Lett. **96**, 407–418 (1990).
14. M. Makhous and Yu. I. Galushkin, "Burial History and Thermal Evolution of the Lithosphere of the Northern and Eastern Saharan Basins," Am. Assoc. Pet. Geol. Bull. **87**, 1623–1651 (2003).
15. M. Makhous and Yu. I. Galushkin, "Burial History and Thermal Evolution of the Southern and Western Saharan Basins. Synthesis and Comparison with the Eastern and Northern Saharan Basins," Am. Assoc. Pet. Geol. Bull. **87** (11), 1–23 (2003).
16. S. Petmecky, L. Meier, H. Reiser, et al., "High Thermal Maturity in the Lower Saxony Basin: Intrusion Or Deep Burial?," Tectonophysics **304**, 317–344 (1999).
17. M. Makhous, Yu. I. Galushkin, and N. V. Lopatin, "Burial History and Kinetic Modelling for Hydrocarbon

Generation. Part I: The GALO Model," Am. Assoc. Pet. Geol. Bull. **81**, 1660–1678 (1997).

18. M. Makhous, Yu. I. Galushkin, and N. V. Lopatin, "Burial History and Kinetic Modelling for Hydrocarbon Generation. Part II: Application of the Model to Saharan Basins," Am. Assoc. Pet. Geol. Bull. **81**, 1679–1699 (1997).
19. J. M. Dautria and A. Lesquer, "An Example of the Relationship between Rift and Dome: Recent Geodynamic Evolution of the Hoggar Swell and of Its Nearby Regions (Central Sahara, Southern Algeria and Eastern Niger)," Tectonophysics **163**, 45–61 (1989).
20. F. Lucazeau, A. Lesquer, and G. Vasseur, "Trends of Heat Flow Density from West Africa", in *Terrestrial Heat Flow and the Structure of the Lithosphere*, Ed. by V. Chermak, L. Rybach, and D. Blackwell (Springer, Berlin, 1990), pp. 417–425.
21. W. Manspeizer, "Separation of Marocco and Eastern North America: A Triassic–Liassic Stratigraphic Record," Geol. Soc. Am. Bull. **90**, 901–920 (1978).
22. R. Guiraud, Y. Bellion, J. Benkhelil, et al., "Post-Hercynian Tectonics in North and West Africa," in *African Geology Reviews. Geological Journal Thematic Issue*, Ed. by P. Bowden and J. Kinnair (Wiley, New York, 1987), pp. 433–466.
23. M. Girod, "Le Massif Volcanique de l'Atakor (Hoggar, Sahara Algerien)," Mem. C. R. Z. A., Série Géologique, No. 12, (1971).
24. M. Megartsi, *Etude des structures circulaires du nord-est d'Illizi (ex Fort-Polignac), Sahara nord-oriental* (Alger, 1972).
25. J. J. Sweeney and A. K. Burnham, "Evolution of a Simple Model of Vitrinite Reflectance Based on Chemical Kinetics," Am. Assoc. Pet. Geol. Bull. **74**, 1559–1570 (1990).
26. M. Makhous and Yu. Galushkin, *Basin Analysis and Modelling of the Burial, Thermal and Maturation Histories in Sedimentary Basins* (TECHNIP, Paris, 2005).
27. N. V. Lopatin, "Temperature and Geologic Time as a Coalification Factor," Izv. Akad. Nauk SSSR, Ser. Geol., No. 3, 95–106 (1971).
28. W. Kalkreuth and M.E. McMechan, "Regional Pattern of Thermal Maturation as Determined from Coal-Rank Studies, Rocky Mountain Foothills and Front Ranges North of Grande Cache, Alberta—Implications for Petroleum Exploration," Can. Petrol. Geol. Bull. **32**, 249–271 (1984).
29. C. M. Bethke, "Modelling Subsurface Flow in Sedimentary Basins," Geol. Rundsch. **78**, 129–154 (1989).
30. C. Clauser and H. Villinger, "Analysis of Conductive and Convective Heat Transfer in Sedimentary Basin, Demonstrated for the Rhein Graben," Geophys. J. Int. **100**, 393–414 (1990).
31. M. Person and G. Garven, "Hydrologic Constraints on Petroleum Generation within Continental Rift Basins: Theory and Application to the Rhine Graben," Am. Assoc. Pet. Geol. Bull. **76**, 468–488 (1992).
32. Yu. I. Galushkin, "Thermal Aureole of an Intrusion and Proposed Mechanism of Its Emplacement into the Sedimentary Sequence of the Cape Verde Rise," Geokhimiya, No. 11, 1197–1205 (1999) [Geochem. Int. **37**, 1079–1086 (1999)].
33. Yu. I. Galushkin, "The Thermal Effect of Igneous Intrusive Bodies on Maturity of Organic Matter—A Possible Mechanism of Intrusion Formation," Org. Geochem. **27**, 645–658 (1997).